DesignCon 2020

How to enforce causality of standard and “custom” metal roughness models

Vladimir Dmitriev-Zdorov, Mentor, A Siemens Business

vladimir_dmitriev-zdorov@mentor.com, +1 720-494-1196

Abstract

Metal roughness is one of the largest contributors to signal loss and dispersion, therefore any design process must use accurate and physically meaningful models of the rough metal. Recent development in this area revealed a deficiency of the existing models related to their non-causality. Papers [3] and [4] proposed causal versions of roughness correction factors for Cannonball-Huray and Hammerstad models. However, these solutions cannot cover a wide class of different metal profiles arising in modern fabrication technology. In this paper we propose a method of enforcing causality of the models given in a form of a table or general functional dependence by way of fitting with a set of causal functions, specifically selected for metal roughness approximation. This method is applied to some standard roughness models (Groiss, Hemispherical, Bushminsky), and custom dependences found from measurements.

Author biography

Dr. Vladimir Dmitriev-Zdorov is a Principal Engineer at Mentor, A Siemens Business. His work includes development of efficient methods of circuit/system simulation, transformation and analysis of multi-port systems, lossy transmission lines, and analysis of SERDES links. The results of his work have been published in numerous papers and conference proceedings.

I. Introduction

PCB design and signal integrity analysis is not possible without considering loss and dispersion caused by materials: dielectric and metal. There exists a consensus about using physically justified causal model of dielectric, such as Djordjevic-Sarkar [1] or its modifications. However, designers realized only recently [2, 3, 4] that causal models of rough metal surface are no less important. For example, [3] proposed a causal version of Huray's roughness model and showed that it increases the group delay of transmission lines and allows better agreement between simulation and measurements. In [4], the authors proposed a mathematical procedure of converting non-causal frequency-dependent loss correction factor (often called *roughness correction factor*) into a causal complex-value correction multiplier, which was illustrated on Cannonball–Huray and Hammerstad models. It was shown that for a given resistive loss, the causal model creates considerably larger internal inductance, which increases both characteristic impedance and phase/group delay of transmission lines.

However, the results and methods considered in [3, 4] solve a relatively narrow class of cases when loss correction is described by simple analytical functions for which Kramers-Kronig integral transformation exists in a closed form. Even some "standard" roughness models, like Hemispherical, Groiss and Bushminsky don't belong to this class. On the other hand, rapidly changing PCB foil fabrication technologies, including electrodeposit and roll-annealing methods, used for different weights an thicknesses, create very different grain structures that require a variety of different roughness models. Oftentimes, the function that describes an increase of loss due to metal roughness is not derived from theory, but is measured post-fabrication on a number of manufactured test structures. The result comes in a form of a table (factor versus frequency), or functional approximation that fits measured points. Such data cannot be used in simulation tools for a number of reasons. First, it is incomplete, because loss increase is just one projection of the roughness phenomena that characterizes losses, but not an internal inductance of the metal. Second, measured data usually ranges from hundred MHz to tens of GHz, but simulation tools need it from DC to about a hundred GHz, as dictated by frequency and time domain analysis resolution and duration.

In practice, to make simulation possible, we need to restore a complete continuous causal complex-value function of frequency that defines a multiplier to the impedance of a smooth metal so that their product correctly describes the complex impedance of the rough metal. Interpolation and extrapolation are methods of restoring "complete" dependence with desirable properties from incomplete or sampled data. Rational fit is an example of interpolation that creates a continuous causal function from a set of frequency points, restores missing imaginary/real part of the dependence from a given real/imaginary part. Unfortunately, rational fit doesn't work well for the functions that describe metal roughness. With smooth metal impedance factored in, the target dependences require fractional power(s) of frequency to accurately describe their asymptotic behavior. Therefore, one of the efforts made in this paper was to find a set of causal basis functions that provide the most compact and accurate representation of the complex roughness correction factor. To allow the desired asymptotic behavior at low and high frequency, we've chosen irrational functions that contain fractional orders of Laplace operator. We used the proposed functional basis to build causal models for Groiss, Hemispheric, and Bushminsky roughness correction factors, and for a number of measured loss dependences.

The paper is organized as follows. Section II discusses the necessary prerequisites and outlines the procedure that applies to roughness dependence given either analytically or by sampled data. In Section III we explain why we need fractional power(s) of complex frequency in our approximation and why such functions make a legitimate set of causal basis functions. We also propose basis functions that work best for the internal complex inductance caused by metal roughness. Sections IV to VI describe the fitting procedure which produces causal versions of the Groiss, Hemispheric and Bushminsky models, and Section VII explains how we can build causal model from measured data. Section VIII compares all five standard models, including causal Cannonball-Huray and Hammerstad found earlier in [4], by using them in a lossy stripline simulation.

II. Roughness correction factor: definitions and how to find it from the loss correction factor

Until recently, most of the sources studying metal roughness used the term "roughness correction factor" [5, 6, 7], by which they meant an increase of metal resistance due to roughness:

$$R_{rough}(\omega) = k(\omega) R_{smooth}(\omega) . \qquad (1)$$

Here, ω is the angular frequency, $R_{smooth}(\omega)$ is frequency-dependent resistance of the smooth metal, which – except for very low frequency – demonstrates square root dependence $R_{smooth}(\omega) \approx R_s \sqrt{\omega}$, in which R_s is a coefficient that depends on physical characteristics of the metal (conductivity and magnetic permeability) and the geometry of the conductor, and $R_{rough}(\omega)$ is the resistance of the rough metal. Factor $k(\omega)$ starts from 1 (no roughness effects at low frequency) and increases with frequency, sometimes reaching 5-7 and beyond. However, in modeling practice, this factor was often applied to both real and imaginary parts of the complex impedance as follows

$$Z_{rough}(i\omega) = k(\omega) Z_{smooth}(i\omega), \qquad (2)$$

thus increasing resistance and internal inductance of the metal in the same proportion. We realize now that this is a mistake, because frequency-dependent real function $k(\omega)$ cannot be causal, and so it makes the complex impedance of the rough metal non-causal, too. As we know [4], expression (2) considerably underestimates the increase of internal metal inductance.

A proper way is to assume that there exists a causal ***complex correction factor*** $K(i\omega) = K_r(\omega) + iK_i(\omega)$ that can be found from the known "roughness correction factor" $k(\omega)$, for which a better name would be either *resistance* or *loss correction factor*. With complex factor in (2), we get

$$Z_{rough}(i\omega) = K(i\omega) Z_{smooth}(i\omega) = K(i\omega)(1+i) R_s \sqrt{\omega} =$$
$$[K_r(\omega) - K_i(\omega)] R_s \sqrt{\omega} + i[K_r(\omega) + K_i(\omega)] R_s \sqrt{\omega} . \qquad (3)$$

As follows from (3), the resistance of the smooth metal is increased by factor $K_r(\omega) - K_i(\omega)$, but the internal inductance is increased by factor $K_r(\omega) + K_i(\omega)$. In [4], they are called respectively ***loss***

correction factor (LCF) and ***inductance correction factor*** (ICF). They both are defined from components of the complex correction factor $K(i\omega)$ (CCF).

What is given to us is a factor $k(\omega)$ in (2), which is the same as $K_r(\omega)-K_i(\omega)$ in (3). How can we restore a complex dependence if we know the difference between its real and imaginary parts? The solution is to define a causal function in which $K_r(\omega)-K_i(\omega)$ comprises either the real or the imaginary part, from which the missing part could be restored. For example, by dividing complex impedance (3) by $i\omega$, we get the complex inductance, which must be a causal function, too:

$$L_{rough}(i\omega)=Z_{smooth}(i\omega)/(i\omega)=[K_r(\omega)+K_i(\omega)]\frac{R_s}{\sqrt{\omega}}-i[K_r(\omega)-K_i(\omega)]\frac{R_s}{\sqrt{\omega}}. \quad (4)$$

It turns out that the imaginary part of the complex inductance is known, because $K_r(\omega)-K_i(\omega)=k(\omega)$. Therefore we only have to restore the missing real part. In [4], we restored it by Kronig-Kramers integral transformation, now we are going to do it by fitting. Once the complex inductance is found, it's possible to find the complex impedance and therefore the complex roughness correction factor.
For convenience, we can introduce frequency-dependent multipliers without initial offset. Factor $K_0(i\omega)=K(i\omega)-1=K_r(\omega)-1+iK_i(\omega)=K_{0r}(\omega)+iK_{0i}(\omega)$ starts from zero, and defines an *additional complex impedance* added by metal roughness as $Z_{rough}(i\omega)=Z_{smooth}(i\omega)+K_0(i\omega)Z_{smooth}(i\omega)$.

III. Fitting the complex inductance: problems and solution

Before we dive into the specifics of particular roughness models, let's see why traditional ways of fitting, e.g. rational fitting, cannot be used for restoring the complex factor $K(i\omega)$ from the imaginary part of the complex inductance (4). Then, we'll choose more appropriate basis functions and use them to find the fit.

Rational fit, why it doesn't work?

The first idea would be to try rational fitting using a set of predefined real or complex poles. For example, by arranging real poles p_m logarithmically within frequency range of interest, we can form and solve a system of N linear equations with respect to coefficients A_m, $m=1...M$

$$imag\left\{\sum_{m=1}^{M}\frac{A_m}{1+i\omega_n/p_m}\right\}=-\frac{1}{\sqrt{\omega_n}}[K_r(\omega_n)-K_i(\omega_n)],\ n=1...N. \quad (5)$$

However, we'll show that this method doesn't work as expected. Figure 1a represents imaginary part of the inductance for the normalized Groiss, Hemispherical and Bushminsky roughness models (red, green and blue curves respectively). The dashed curve is the imaginary part of a single rational term with pole $p=1$. All imaginary parts are taken with opposite sign to make them positive and allow logarithmic scale along vertical axis.

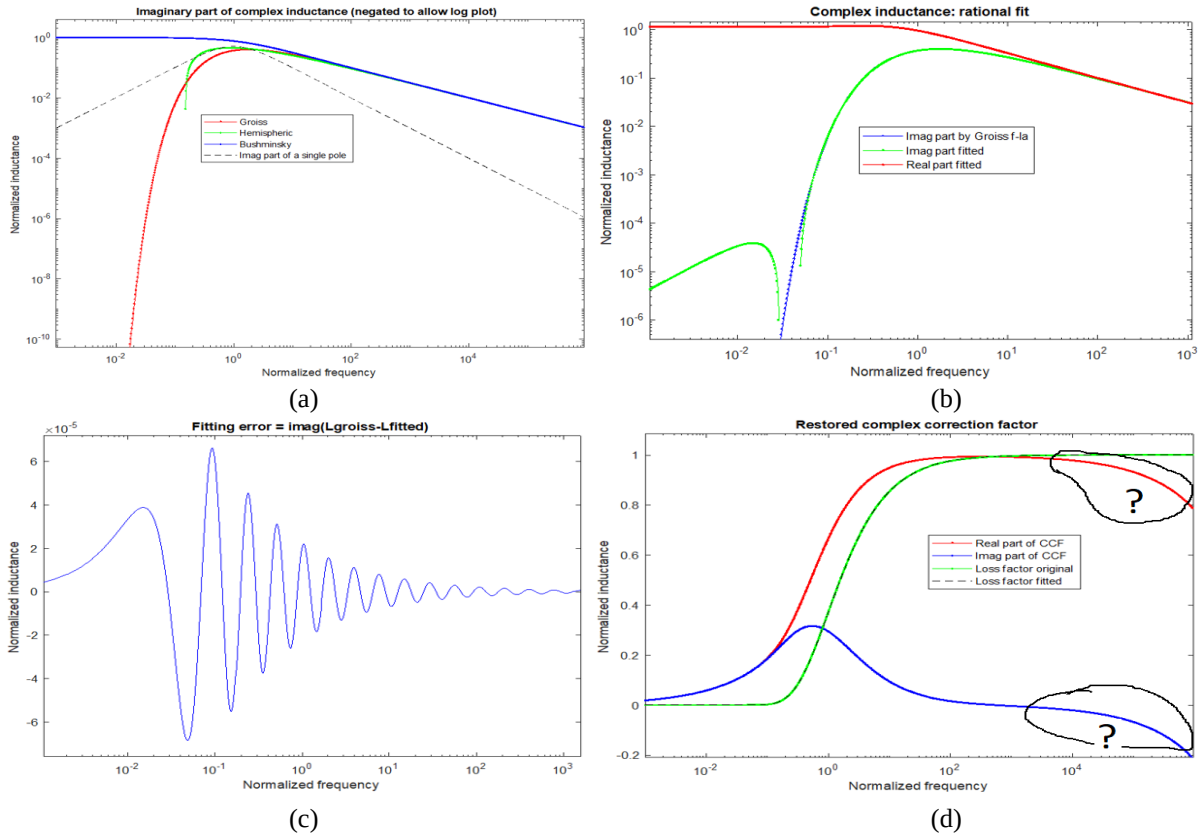

Figure 1. Log/log plot of the imaginary part of the complex inductance for Groiss (red), Hemispherical (green) and Bushminsky (blue) roughness models, and a single rational pole (dashed black) (a). Fitting complex inductance of Groiss model (blue) by a set of 50 real poles (green, red), (b). Fitting error (c), and the restored real/imaginary parts of the complex correction factor (d)

The asymptotic behavior of a single pole in Figure 1a considerably differs from other curves. It starts growing linearly with frequency, but after the peak decreases in inverse proportion to it. The imaginary parts of the inductance derived from standard roughness models initially grow with very different rates (or even don't grow), but then they all decrease as $1/\sqrt{\omega}$. Despite the difference in asymptotic behavior, we hope to achieve accurate approximation by taking sufficiently many poles in (5). For example, fitting the normalized complex inductance $L_{rough}(i\omega)$ for the Groiss model with 50 poles gives us, though not perfect, but reasonable accuracy (Figure 1b). The error, defined as the difference between the given and fitted imaginary parts is shown in Figure 1c. It doesn't exceed 1e-4. Indeed, we were able to fit loss correction factor accurately (Figure 1d, green). However, the real and imaginary parts of the restored complex correction factor (CCF) on the same plot don't look correct. We expected them to flatten at high frequency like the loss correction factor, but instead they are both going down. Why? Remember, that the loss correction factor (3) is the difference between the real and imaginary parts of CCF. If we modify the real and imaginary parts of CCF by adding the same function, the difference won't change. Since we found our solution by fitting, such addition must be a causal function. What causal function's real and imaginary parts are identical? It could be anything containing the terms $\sqrt{i\omega}$. In other words, fitting with rational poles is "blind" to such errors if they appear in CCF, because (a) it is

basically unable to accurately represent fractional powers of complex frequency, and (b) even a tiny error that contains $\sqrt{i\omega}$ will destroy the asymptotic behavior of CCF.

Fitting with fractional powers of complex frequency

From $\mathrm{imag}\left\{L_{rough}(i\omega)\right\}$ dependences, shown in Figure 1a, we see that the rate of growth could be variable, starting from extremely steep, then flattening, before the function turns down and decreases as $1/\sqrt{i\omega}$. To describe such behavior, the functions need to contain fractional powers of frequency, possibly different fractional powers, to represent a variable growth rate. However, defining such functions is not an easy task. We need to answer the following questions: (a) what fractional powers of $s^{\alpha} = (i\omega)^{\alpha}$ make causal functions, (b) what functions in s^{α} make passive contribution into $L_{rough}(s)$ (by keeping its imaginary part negative, which corresponds to positive loss in complex impedance), and (c) how to ensure "delay-causality" of the model, meaning that the real part of the internal inductance added due to roughness must remain non-negative (i.e. roughness may only increase the delay of the conductor).

Are fractional powers of $s = (i\omega)$ causal?

Fortunately, the answer is yes, and it follows from fractional calculus [8, 9], a remarkable by not widely known branch of mathematics, and from the nature of Laplace transformation. In particular, fractional calculus operates with fractional orders of integral and differential operators that exist for some "proper" functions. Let's take the function $f(x)$ that exists for all $x \geq 0$ and define its first-order integral as $(Jf)(x) = \int_0^x f(v)dv$; integral of the second order as $(J^2 f)(x) = \int_0^x \left(\int_0^v f(u)du \right) dv$, and so on. The *Cauchy formula* [10] is known to compress multiple integrations into a single integral as $(J^n f)(x) = \frac{1}{(n-1)!}\int_0^x (x-v)^{n-1} f(v)dv$. The latter could be generalized onto non-integer powers by formally replacing the integer parameter n with real α which makes

$$(J^{\alpha} f)(x) = \frac{1}{\Gamma(\alpha)}\int_0^x (x-v)^{\alpha-1} f(v)dv. \qquad (6)$$

Such generalization works for the functions for which the integral (6) exists for any $x > 0$. If the function $f(v)$ is zero for all $v < 0$, it can be considered as an impulse response of a causal system. Then, integral (6) will be zero for all $x < 0$, thus describing a causal system, too.

Fractional derivatives can be defined as operations inverse to fractional integrals. As we know, multiplication or division of the Laplace transform $F(s)$ by complex frequency s, is equivalent to differentiation or integration of the original, respectively. If fractional integrals and/or derivatives exist, and the original "time domain" function $f(t)$ is causal then $s^{\alpha}F(s)$ and $s^{-\alpha}F(s)$, and the respective Laplace operators s^{α} and $s^{-\alpha}$ should represent causal functions as well.

If $s = ix$ and $x \geq 0$ then the fractional order operaor is $s^\alpha = x^\alpha e^{i\frac{\pi\alpha}{2}} = x^\alpha (\cos\frac{\pi\alpha}{2} + i\sin\frac{\pi\alpha}{2})$. Realness of a causal function implies that $(s^*)^\alpha = \left[s^\alpha \right]^*$, hence we can use $s^\alpha = |x|^\alpha (\cos\frac{\pi\alpha}{2} + i\,\mathrm{sign}(x)\sin\frac{\pi\alpha}{2})$ for positive and negative x. Figure 2 shows the trajectories of s^α on the complex plane (a), and the dependency of the imaginary parts s^α on frequency (b). The trajectories (a) are straight lines indicating that the ratio between real and imaginary parts depend on power, but not on frequency. Figure 2(b) implies that the steepest dependency can be achieved with power close to 1. We do not consider cases with $\alpha > 1$ because real part of the complex inductance must remain non-negative.

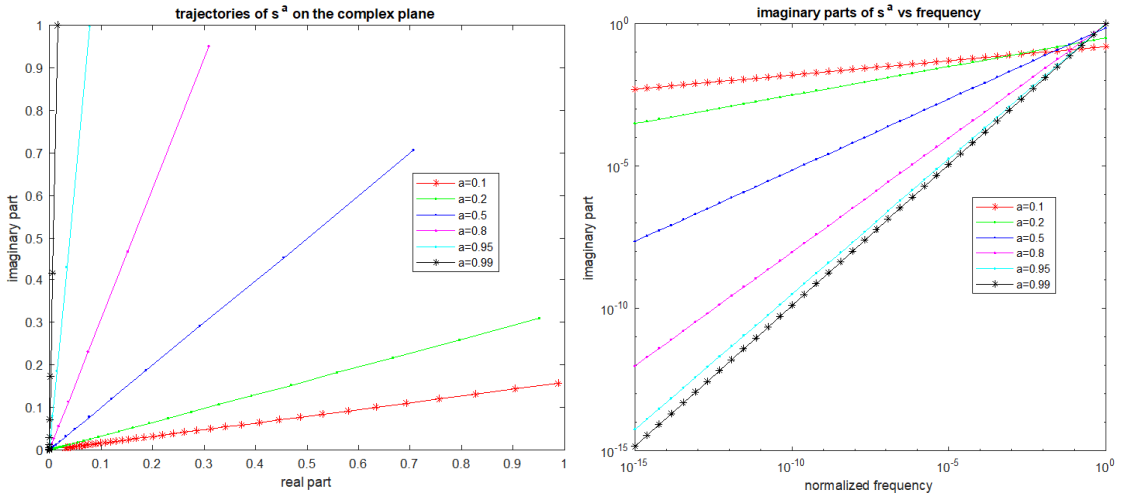

(a) (b)

Figure 2. Fractional powers of complex frequency s^α. Trajectory on the complex plane (a) and dependency of imaginary parts (b)

If fractional powers s^α are causal functions, then many analytical functions of complex argument $f(z)$ create causal functions of the form $f(s^\alpha)$. The exceptions are those for which inverse Laplace integral doesn't exist.

Choosing the appropriate basis functions

Of course, complex inductance (4) must be finite and decreasing to zero at high frequency, because of the multiplier $1/\sqrt{\omega}$. To make this possible, we suggest using formula

$$y(s,\alpha) = \left(1/s^\alpha\right)\arctan(s^\alpha), \qquad (7)$$

that contains Laplace operators of fractional order $\alpha \in (0,1)$. Inverse Laplace transform of (7) can be represented by a convolution of fractional powers of time t and the term $t^{\alpha-1}E_{\alpha,\alpha}(-\alpha t^\alpha)$, where $E_{\alpha,\beta}(z)$ is Mittag-Leffler function. Since all components of the convolution are identically zero for $t < 0$, so is the time domain equivalent of (7).

By increasing α, it is possible to make the imaginary part grow steeper, however, it will be decreasing faster after its peak as well. Figure 3 shows a set of functions (7) with different values of α.

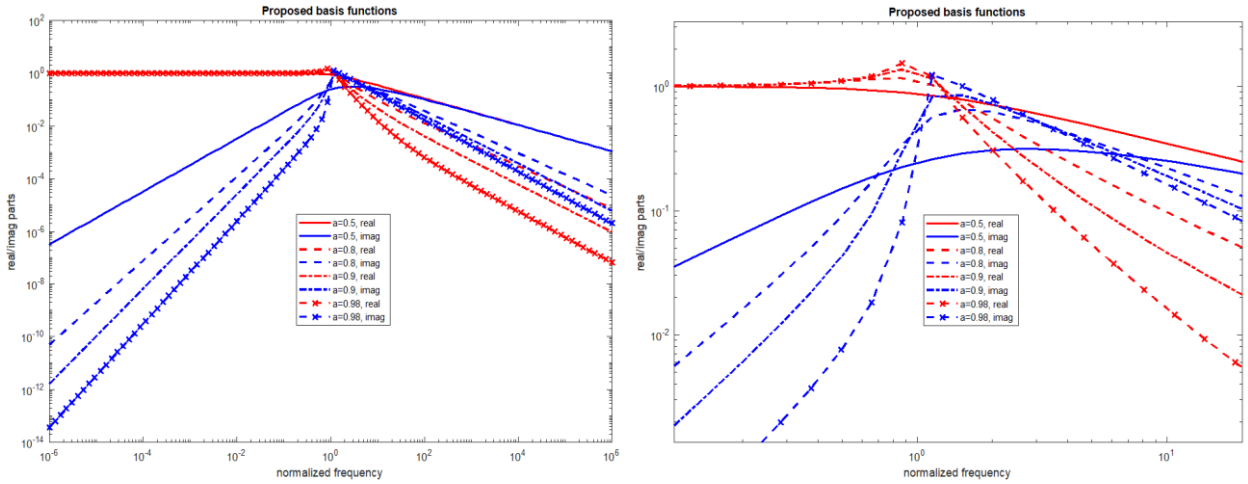

(a) (b)

Figure 3. The proposed basis functions (imaginary part is negated to allow logarithmic plot). Plot (b) is a zoomed version of (a), to show behavior near the peak

The slope of the (negated) imaginary part at very small frequency is approximately 2α, or factor $10^{2\alpha}$ growth per decade. For $\alpha > 1$ the sign of the imaginary part oscillates and the function cannot be used as a fit basis. However, the useful feature of these basis functions is the fact that just before the peak, the imaginary part becomes increasingly steep when α approaches to 1. This seems to be useful when representing the Groiss and Hemispherical models (see Fig.1a). To model a curve with increasing steepness, it is possible to combine the components with higher power (at lower frequency) with increasingly smaller powers thereafter, while keeping them above (or equal) 0.5.

With the new basis functions, our fitting problem reduces to equation:

$$L_{im}(x) \approx \mathrm{Im}\left[\sum_{m=1}^{M} A_m \left(\frac{p_m}{s}\right)^{\alpha_m} \arctan\left(\frac{s}{p_m}\right)^{\alpha_m}\right]. \qquad (8)$$

The goal is to find a set of coefficients A_m for a chosen set of "poles" p_m and associated powers α_m. As before, the pole frequencies p_m can be distributed logarithmically in the frequency range of interest. The powers should gradually decrease from e.g. 0.98 to 0.5 as we go from low to high frequency poles. It is also possible to assign several components with identical poles, but different powers; accurately found solution - e.g. by singular value decompositions methods - will result in a proper combination of them.

IV. Building Causal Groiss Roughness Model

As shown in [11, 5], the normalized roughness correction factor of the Groiss model (or loss correction in the proposed terminology) has the form:

$$F_g(\Delta_i, \delta_s) = \exp\left[-\left(\frac{\delta_s}{2\Delta_i}\right)^{1.6}\right], \qquad (9)$$

where Δ_i is the roughness bump size (*rms*), and $\delta_s = (\pi f \mu\sigma)^{-1/2}$ is the skin depth. As skin depth decreases with frequency, this factor changes from zero to 1. Therefore it is a normalized factor describing an additional loss due to metal roughness.

By introducing normalized frequency $x = 2\omega\mu\sigma\Delta_i^2$, we get:

$$K_{g0}(x) = \exp(-1/\sqrt{x^{0.8}}) . \qquad (10)$$

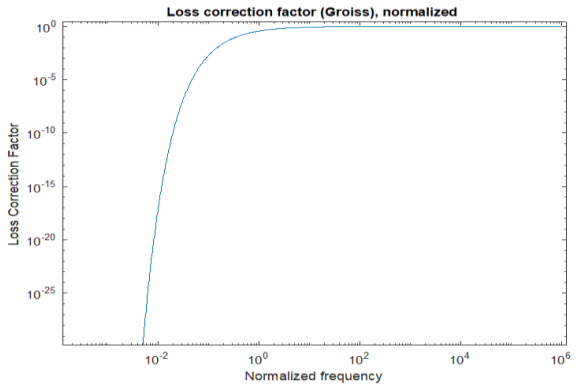

(a)

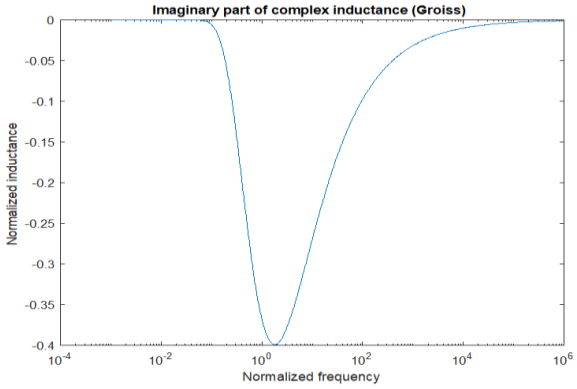

(b)

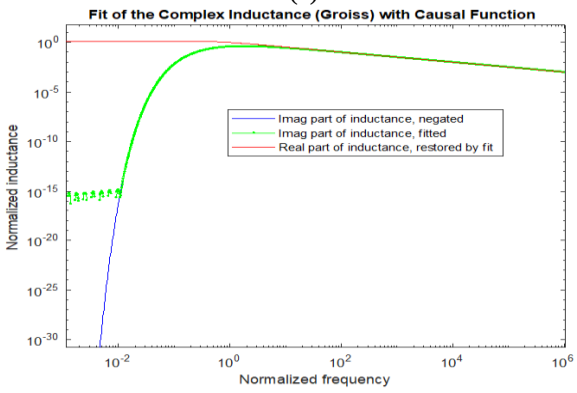

(c)

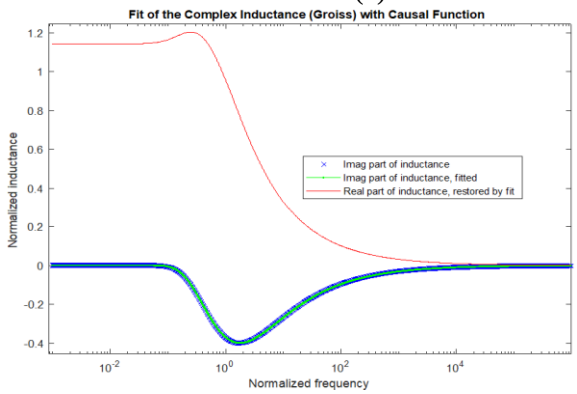

(d)

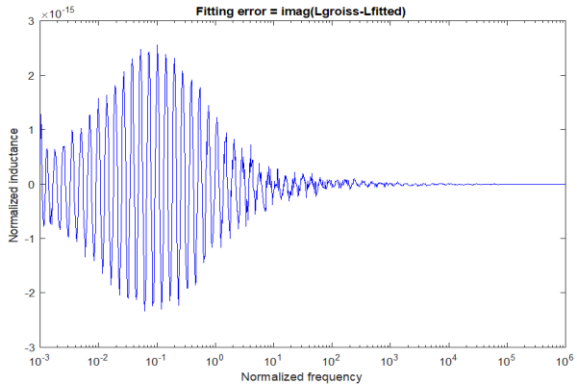

(e)

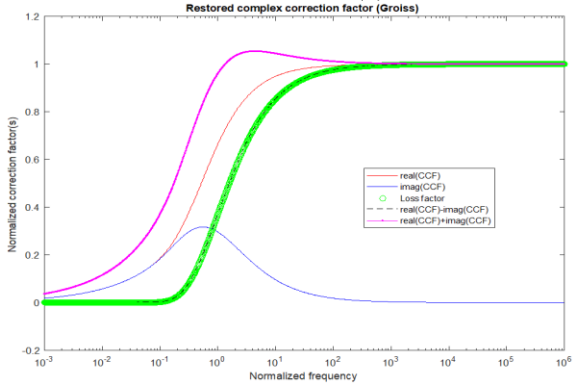

(f)

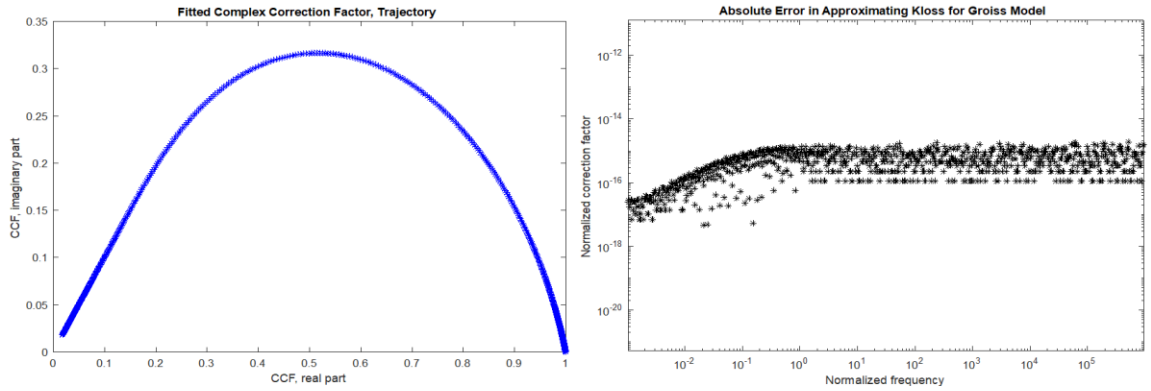

(g) (h)

Figure 4. Restoring the causal Groiss model. Normalized loss correction factor in log scale (a); imaginary part of the additional complex inductance (b); fit of the complex inductance together with restored real part (c); restored complex inductance with "natural" vertical scale (d); absolute fitting error for the inductance (e); restored CCF (thin red/blue), loss correction factor, original (green), and its fit (dashed black), and inductance correction (magenta) (f); trajectory of the CCF (g); and absolute error approximating loss correction factor (h)

As explained in Section II, the loss correction factor (LCF) $K_{g0}(x)$ equals the difference between real and imaginary parts of the unknown complex correction factor. LCF is shown in Figure 4a. It is practically zero below $x < 10^{-2}...10^{-1}$ but then steeply goes up and flattens at 1. The imaginary part of the normalized complex inductance (b) is LCF divided by $\sqrt{x}$ and taken with sign minus. Figure 4c shows the imaginary part of the inductance, computed (blue) and fitted (green) by solving equations (8). For convenience, both are shown in logarithmic scale, which requires opposite sign. The red curve is the real part of the inductance restored by fitting. Figure (d) shows them with conventional sign and scale; we can see that the real part of the inductance peaks at about $x \simeq 0.3$. In this respect, it is similar to Hammerstad model [4]. The fitting error for the complex inductance is shown in (e): it remains below 1e-15. Multiplication of the normalized complex inductance by ix gives us the complex impedance (normalized), added due to roughness. By dividing the result by $\sqrt{2ix}$ (with factor 2 because in (3) we used $(1+i)$ instead of $(1+i)/\sqrt{2}$), we find the complex correction factor (CCF), (f). The real and imaginary parts of CCF grow initially as $\sqrt{x}$ thus making the difference, i.e. loss correction factor, practically zero. However, an inductance correction factor (magenta) equals the sum of the real and imaginary parts of CCF, and is way larger than the loss factor. We observe a perfect fit for the loss correction factor (black versus green). The trajectory plot of the CCF (imaginary part versus real) is shown in (g), and the absolute difference between the original loss correction factor and its restored version is in (h). The error remains at about 1e-15, which is close to the limit for double precision.

V. Causal Hemispherical Roughness Model

The normalized form of Hemispherical "roughness factor" is given in [5, 6, 7] as:

$$F_h(r_i, \delta_s, k) = \frac{2\delta_s}{\pi r_i^2}\,\mathrm{Abs}\left\{\mathrm{Re}\left[\frac{3\pi\eta}{4k^2}(\alpha(1)+\beta(1))\right]\right\} - \frac{1}{2}, \qquad (11)$$

In which the negative values at low frequency should be replaced by zero. In (11), δ_s is skin depth, r_i is the radius of hemispheres approximating metal profile, and $\eta = \sqrt{\mu_0/(\varepsilon_0\varepsilon')}$. Factor k is inverse to wavelength in dielectric, and proportional to frequency. The complex frequency-dependent components

$\alpha(1), \beta(1)$ are defined in [6, 7]. Skin depth decreases as $\sim 1/\sqrt{f}$, and the multiplier in the brackets decreases as $\sim 1/f^2$. However, the overall growth occurs due to proportionality $\alpha(1) \sim f^3$.

It is difficult to make the Hemispherical model a function of a single normalized frequency, because parameters η and k depend on relative permittivity of dielectric, which is also frequency-dependent. For that reason, we'll build the dependence using the method defined in [7] assuming $\varepsilon' = 3.7$ and $r_i = 1\mu m$, then rescale it when comparing to normalized models of other types. Another problem here is that the model (11) diverges at high frequency due to fast growing term $\alpha(1)$. For the purpose of fitting, we need the dependence to be defined over a wide range, but asymptotically approaching a finite value at high frequency. This is achieved by extrapolating the dependence above 100GHz, as shown in Figure 5a.

It is also necessary to "pre-process" the data to remove the discontinuity of derivative at cut-off frequency (around 3GHz), because we cannot accurately approximate such dependence with smooth causal functions (8). Despite smoothing, an initial rising portion remains the "steepest" for higher derivatives, and we may need to add more poles in its vicinity to achieve better accuracy.

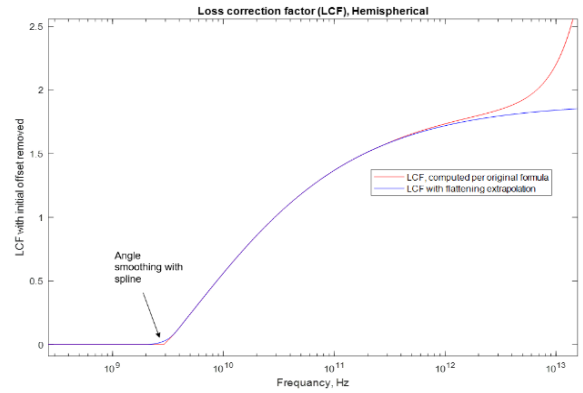

(a)

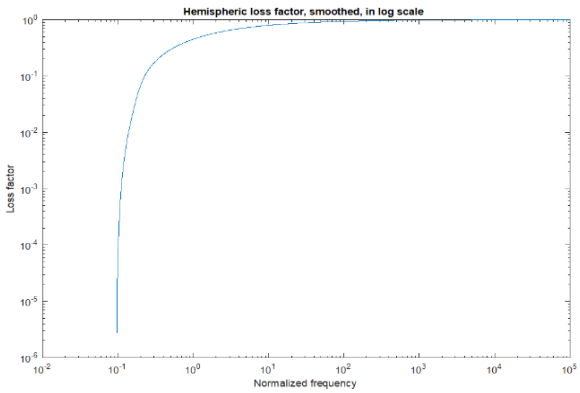

(b)

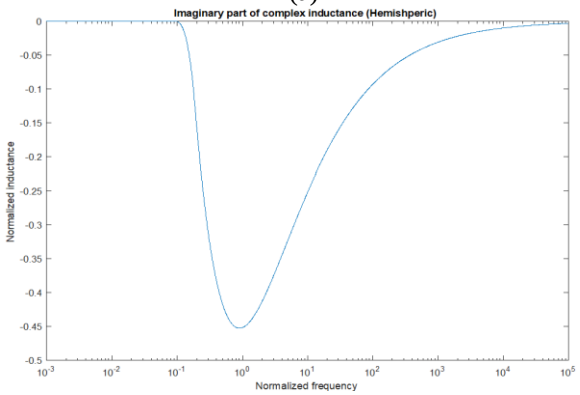

(c)

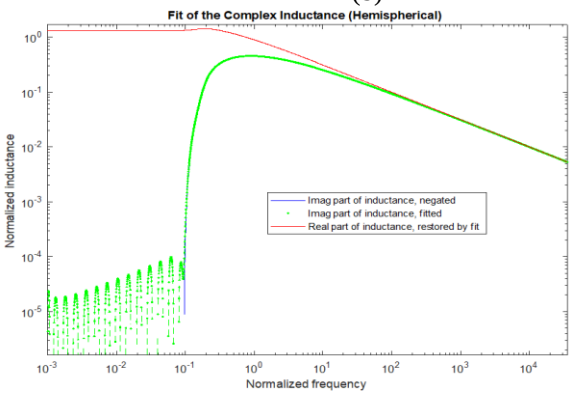

(d)

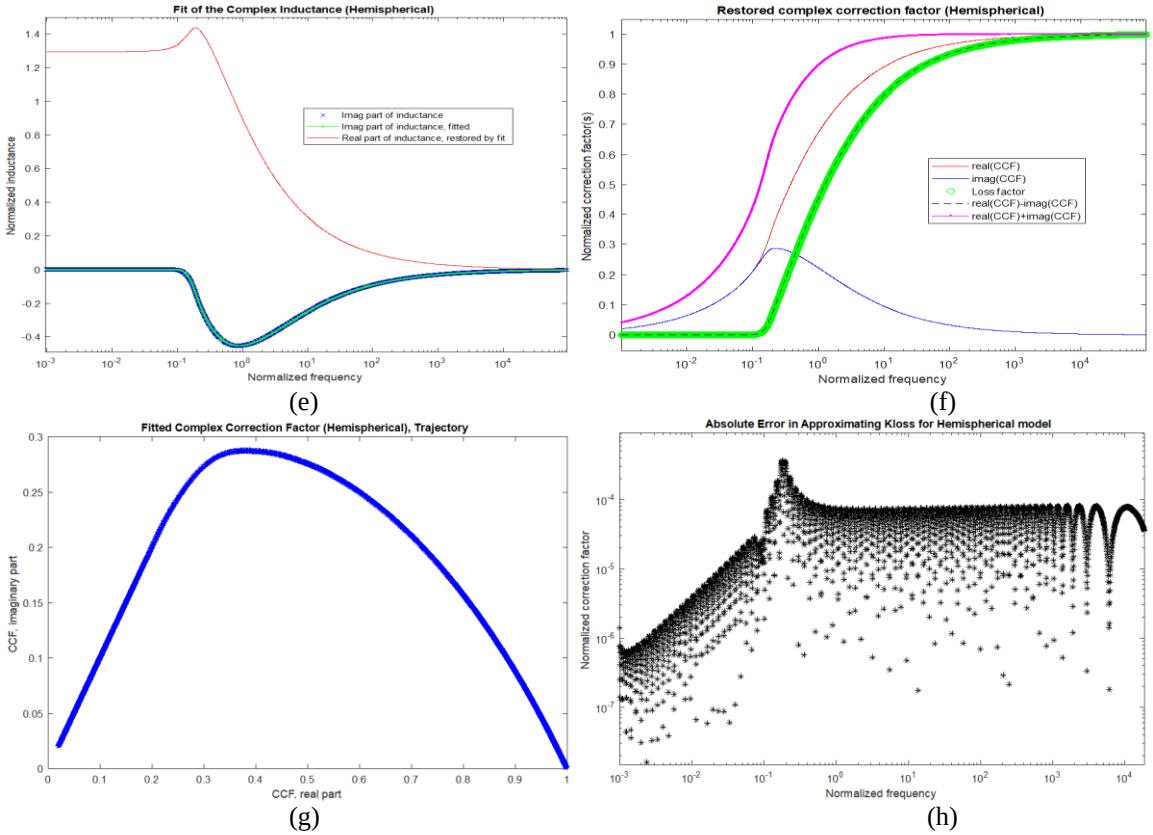

Figure 5. Loss correction factor found by formula (11) (red), and modified by extrapolation at high frequency and spline smoothing at cut-off (blue) (a); modified loss correction factor in log scale (b); imaginary part of the complex inductance (c); complex inductance fitted (d), with its real part restored (d); complex inductance in "natural" scale (e); restored complex factor, loss and inductance correction factors (f); trajectory plot of the complex factor (g); and absolute error when fitting loss correction factor (h)

Figure 5b depicts the normalized loss factor in logarithmic scale, as a function of normalized frequency ($x = 1$ corresponds to 20GHz). Figure 5c shows the imaginary part of the complex inductance, 5d shows the same curve in logarithmic scale, negated (blue) with its fit using formula (8) (green), and the restored real part of the complex inductance (red). As we see, the fitting accuracy is about 1e-4. It's much worse than what we achieved for the Groiss model. The error is caused by the non-smooth behavior of the original dependence, which can be eased by spline interpolation of the cut-off region, but not remove discontinuity of higher derivatives. By making the interpolating interval wider, we may reduce fitting error, however what we get may not be exactly the dependence we need. The complex inductance in natural scale (Figure 5e) demonstrates the prominent peak of the real part, which corresponds to the point of discontinuity. However, the exact magnitude of this peak depends on the "sharpness" of the take-off area after spline interpolation. Figure 5f shows the restored complex correction factor (red/blue), loss correction, original (green) and fitted (black), and inductance correction factor (magenta). Figures 5g and h demonstrate the trajectory of the complex factor and fitting error for the loss correction factor. Apart from considerably larger error, the results for Hemispherical model are similar to Groiss. For example, the real and imaginary parts of the complex correction factor remain practically equal for $x < 0.1$. In this region, we don't observe resistive loss yet, however, the inductance

added due to metal roughness is already considerable. Also, since the real and imaginary parts of CCF remain equal, the initial portion of the trajectory is practically a straight line.

VI. Causal Version of Bushminsky Roughness Model

The normalized form of Bushminsky "roughness factor" is given in [5] as:

$$F_B(\Delta_i, \delta_s) = \tanh\left(\frac{\Delta_i}{1.8\delta_s}\right), \qquad (12)$$

where the parameters are the same as in the Groiss model (9). By choosing normalized frequency $x = \frac{200}{81}\omega\mu\sigma\Delta_i^2$, we turn (12) into the normalized loss correction factor

$$K_{B0}(x) = \tanh(\sqrt{x})\,. \qquad (13)$$

It is shown in Figure 6a. Now, let's follow the same procedure as we did for the Groiss and Hemispherical model. Imaginary part of complex inductance is $\text{imag}\{L(ix)\} = -K_{B0}(x)/\sqrt{x}$. Remarkably, at low frequency we get $\text{imag}\{L(ix)\} = -1$ (see Figure 6b), as follows from the fact that for small x $\tanh(\sqrt{x}) \approx \sqrt{x}$. With non-zero imaginary part at low frequency, the real part has to grow unlimited towards DC, approximately like $|\log(x)|$, which is illustrated by Figure 6c. The fitting error is reasonable (below 1e-6) but as expected, it increases toward low frequency as the function itself. The restored real and imaginary parts of the complex factor (CCF) are shown in Figure 6f, together with the computed inductance correction factor and the fitted LCF. Unlike the Groiss and Hemispherical models, the real and imaginary parts of CCF are separate from the start, because LCF doesn't have an initial zero pedestal. This model also has the smallest imaginary part of CCF which brings the LCF and inductance correction factor closer to each other. Hence, non-causal version of Bushminsky model appears "less non-causal" than the similar dependence for Groiss or Hemispherical. The trajectory plot, Figure 6g, is tilted towards higher resistive losses, because due to unbounded inductance at low frequency, the factors grow and decay with different speeds. The overall fitting error for LCF is below 1e-9.

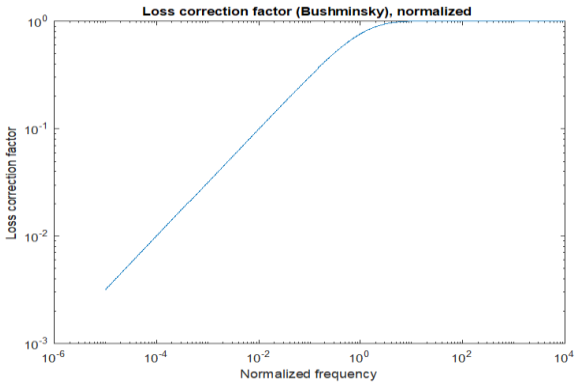

(a)

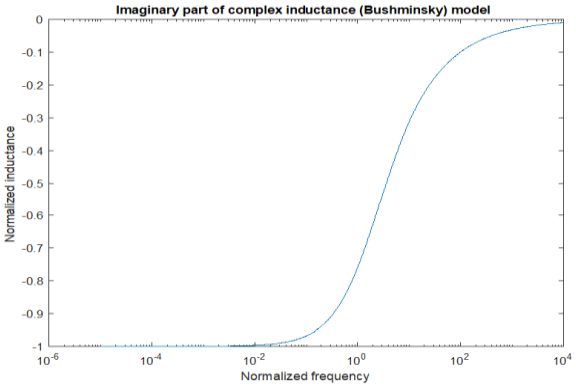

(b)

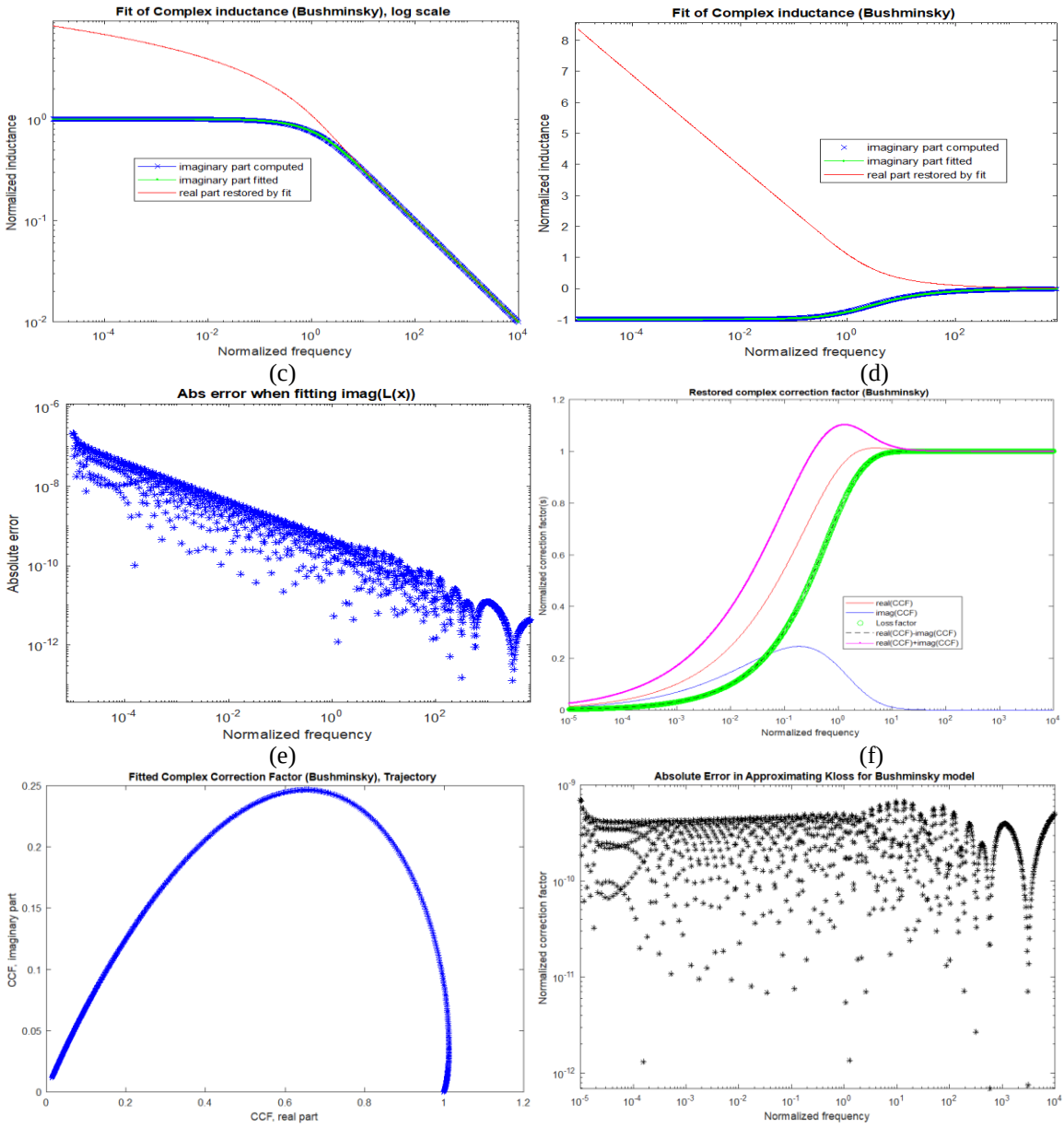

Figure 6. (a) Loss correction factor described by (13) in logarithmic scale; (b) imaginary part of complex inductance; (c) complex inductance fitted in log scale, real (red) and imaginary (blue); (d) complex inductance, natural scale; (e) absolute error when fitting complex inductance; (f) restored real and imaginary parts of the complex factor (red, blue), loss (green) and inductive (magenta) correction factors; (g) trajectory plot of the complex factor; (h) absolute error when fitting loss correction factor

VII. Extracting Causal Roughness Model from Measured Data

The main approach stays the same: find the complex inductance added due to metal roughness by solving equations (8). However, we have to do some additional steps to find the frequency-dependent loss factor from given S-parameters. We'll use a measured and de-embedded 6-inch stripline model, same as in [4]. The two-port S-parameters are shown in Figure 7a.

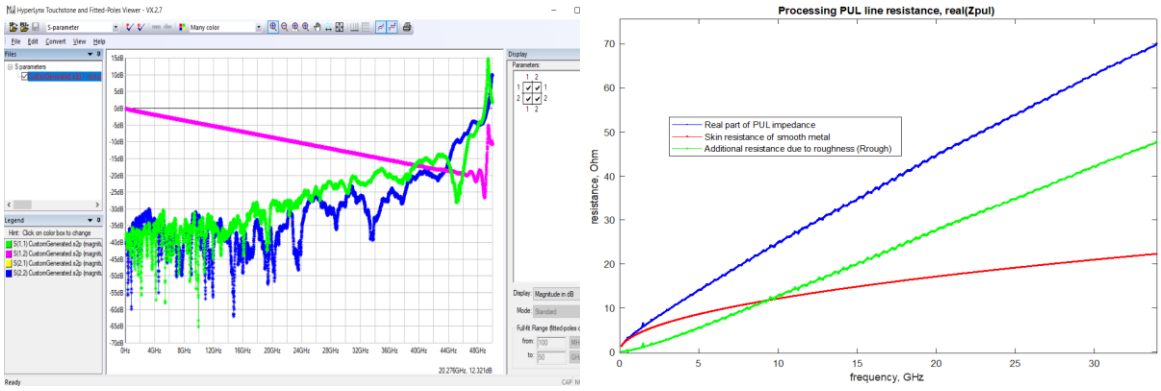

(a) (b)

Figure 7. (a) Measured & de-embedded S-parameters; (b) extracted PUL resistance times T-line length (blue), "smooth" metal resistance (red), and additional resistance added due to metal roughness (green)

A script was used to find the propagation operator and characteristic admittance from measured S-parameters, and then extract the bulk per-length impedance (BPLI, which is PUL impedance times the line's length), and the line's BPLI conductance. Figure 7b shows the real part of such impedance (blue curve). The imaginary part of the impedance is dominated by a large contribution from external inductance therefore is not very convenient for roughness characterization. Since the dependence starts from tens of MHz, it is possible to find such value R_s that makes the curve describing $R_s\sqrt{f}$ (shown red) tangent to BPLI at low frequency. The difference between them (green) is an additional resistance added due to metal roughness. The ratio between this additional resistance and $R_s\sqrt{f}$ gives us a loss factor $K_0(f)$ that doesn't have an initial offset.

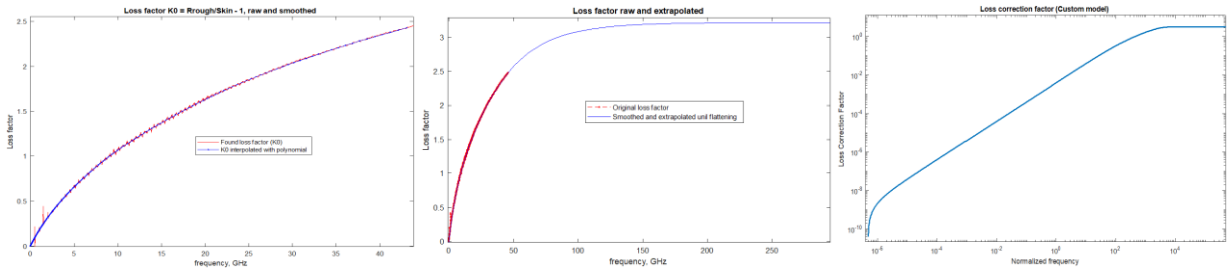

(a) (b) (c)

Figure 8. (a) Found loss factor, raw (red) and interpolated (blue); (b) raw (red) and interpolated/extrapolated loss factor (blue); (c) wide-band loss factor versus normalized frequency, logarithmic scale

The $K_0(f)$ we found is shown in Figure 8a (red), together with its interpolation (blue). To proceed with fitting, we need to extend the dependence until it settles at a certain level, which is shown in Figure 8b (blue curve). Finally, we make it a wideband function of a normalized frequency, as shown in Figure 8c. The following steps are practically identical to those of standard models.

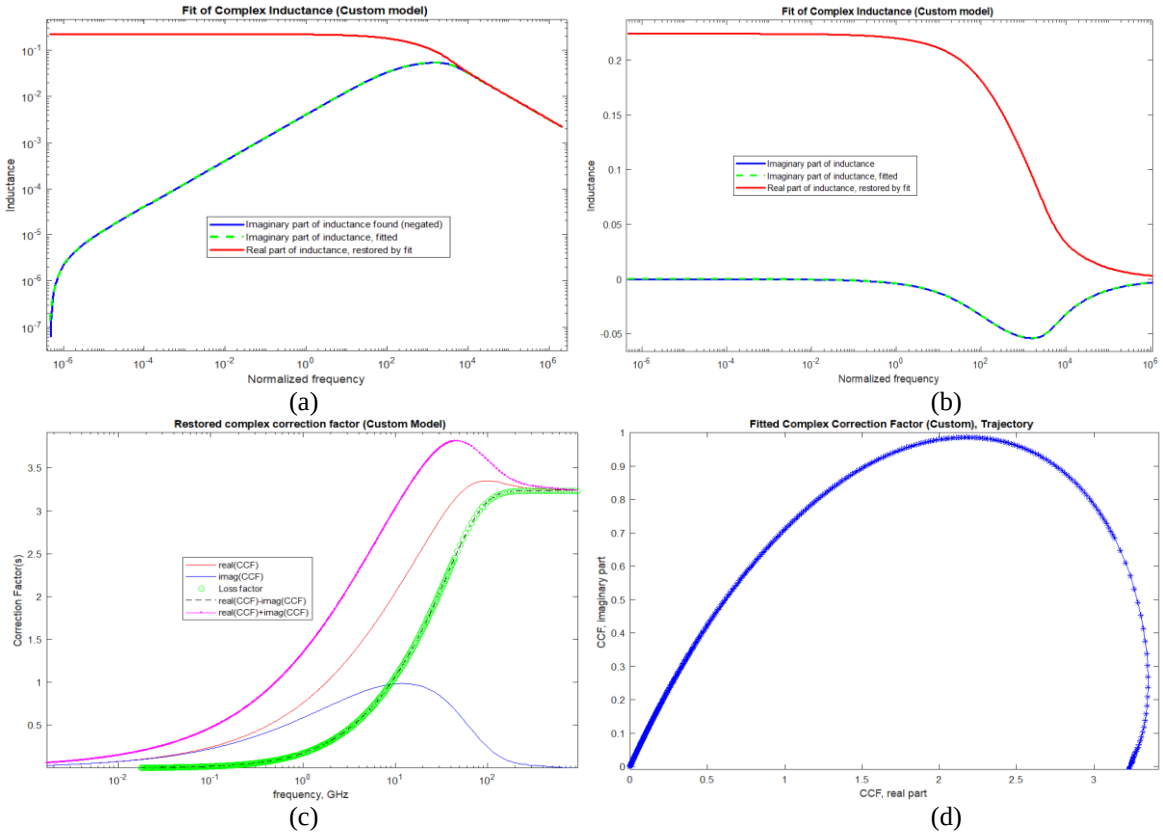

Figure 9. (a) Imaginary part of inductance (blue, shown as positive), its fit (dashed green) and restored real part of inductance (red); (b) restored complex inductance, natural scale; (c) restored real and imaginary parts of the complex factor (red, blue), loss (green) and inductive (magenta) correction factors; (d) trajectory plot of the complex factor

Figure 9 illustrates the process of fitting. By dividing the loss factor by the square root of frequency and taking the result with opposite sign, we find the imaginary part of the internal inductance added due to metal roughness. This is shown in Figure 9a (blue), for convenience with opposite sign. Fitting (8) approximates the imaginary part of inductance (dashed green) and restores its real part (red). The absolute fitting error doesn't exceed 1e-4. Figure 9b shows the restored complex inductance with natural scale and sign, same denotations. The restored complex correction factor (CCF) is in Figure 9c (red and blue curves), magenta and green are the inductance and loss correction factors, respectively. Figure 9d shows the trajectory of CCF on the complex plane as frequency changes from zero to infinity. This CCF is not normalized so its real part goes up to ~3.23.

VIII. Comparison of causal standard models

Normalized Roughness Factors

Here we compare the computed dependencies to each other, together with analytical solutions found earlier in [4] for the Cannonball-Huray and Hammerstad models. This comparison is somewhat similar to [5], but for causal models. Figure 10 shows the real and imaginary parts of the complex correction factor (CCF) for "standard" models. The dependencies, shown as solid curves, are real parts; they don't have initial offset and change from 0 to 1. The imaginary parts are drawn with dashed lines of the same color. Frequency is normalized as well. To use them in analysis, the dependencies must be scaled

vertically by magnitude and horizontally along frequency axis, as required by metal profile or fitting to measurements. The resulting scaling factor becomes a complex multiplier at the impedance of a smooth metal so that the product is an additional impedance added due to metal roughness.

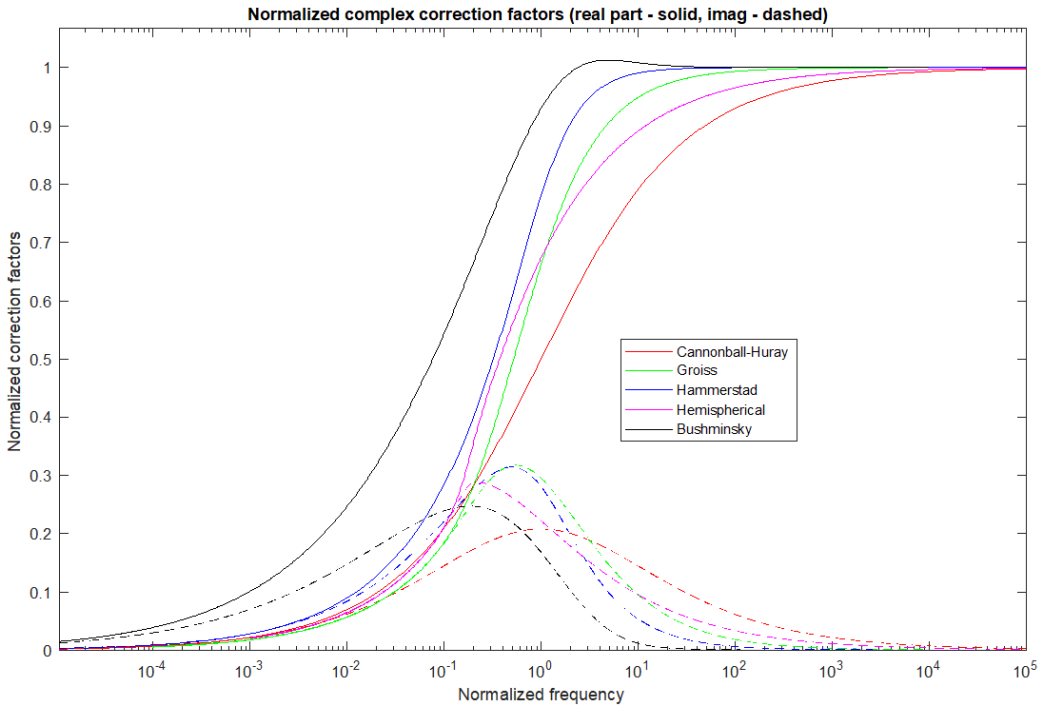

Figure 10. Normalized complex correction factor for the five "standard" models: Cannonball-Huray, Groiss, Hammerstad, Hepispherical and Bushminsky. Real parts are shown with solid lines, imaginary – dashed of the same color

It is important to see how close the real and imaginary parts are initially, and how large imaginary part is compared to real. The first characterizes loss due to roughness, because the difference between the real and imaginary parts is the loss correction factor. For example, we can see that the real and imaginary parts are very close initially for the Groiss (green) and Hemispherical (magenta) models. This initial region is where the loss factor stays at zero level. These two models also have the largest imaginary part that makes the loss and inductance correction factors quite different. On the other hand, in the Bushminsky model the real and imaginary parts are distant from the start, indicating that resistive loss starts at low frequency. Also, the Bushminsky model is the only one for which the real part of the factor peaks, and so does the inductance correction factor, although the loss factor remains monotonic. The imaginary part of the factor is what creates the difference between the loss and inductance correction factors (they differ by two times the imaginary part). Since a non-causal model assumes the same multiplier at the resistive and inductive portions of the impedance, the ratio between the imaginary and real parts could be a measure of "inaccuracy" of a non-causal model. For example, in the Groiss and Hemispherical models real and imaginary parts separate late, where the latter is considerable. For this reason, these models have minimal loss at low frequency but unusually large inductance factor. This also means that the non-causal versions of the Groiss and Hemispherical models are least accurate since they underestimate inductance the most. By these features, the Cannonball-Huray and Hammerstad models can be ranked between the Bushminsky and Groiss/Hemispherical.

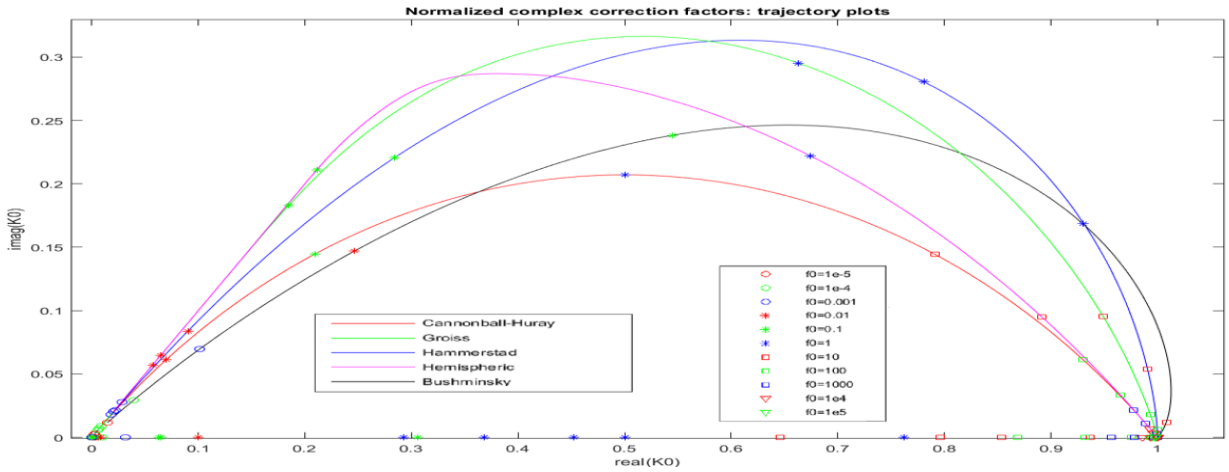

Figure 11. CCF represented as trajectory on the complex plane. Curves have the same colors as in Figure 10, normalized frequencies are designated with colored symbols.

Figure 11 shows CCF trajectories on the complex plane. Since causal functions demonstrate clockwise curving of the trajectory as frequency goes from zero to infinity, the imaginary part of CCF is always non-negative. This also agrees with physics: a non-smooth metal profile increases magnetic field created by the current and so it does for internal inductance. As we see, for the Groiss and Hemispherical models the trajectory starts as a straight line, under 45 degree angle, indicating that both real and imaginary parts are equal and grow as $\sqrt{f}$. The Bushminsky model has the smallest slope at low frequency, while the Cannonball-Huray and Hammerstad models are in between.

Another interesting characteristic is model symmetry at low and high frequencies. Cannonball-Huray (red) is an arc of a circle cut by the right angle. It has identical slopes at low and high frequencies. The imaginary part reaches maximum when the normalized frequency is 1 and real part is half way between zero and its maximal value. The Groiss model is quite symmetrical as well. The Hemispheric model is tilted towards low frequency, while the Hammerstad and especially Bushminsky models are tilted towards higher frequency. Trajectories of the non-causal versions of the same models are all located within segment [0,1) on the real axis. At all frequencies, a non-causal factor is real and equals the loss factor.

The next plot (Figure 12) is a trajectory that shows how the loss and inductance correction factors change over frequency. Since the loss and inductance factors are the difference and the sum of real and imaginary parts of CCF, respectively, they are related by congruent transformation and therefore the plot in Figure 12 is a copy of trajectory from Figure 11 rotated by 45 degrees.

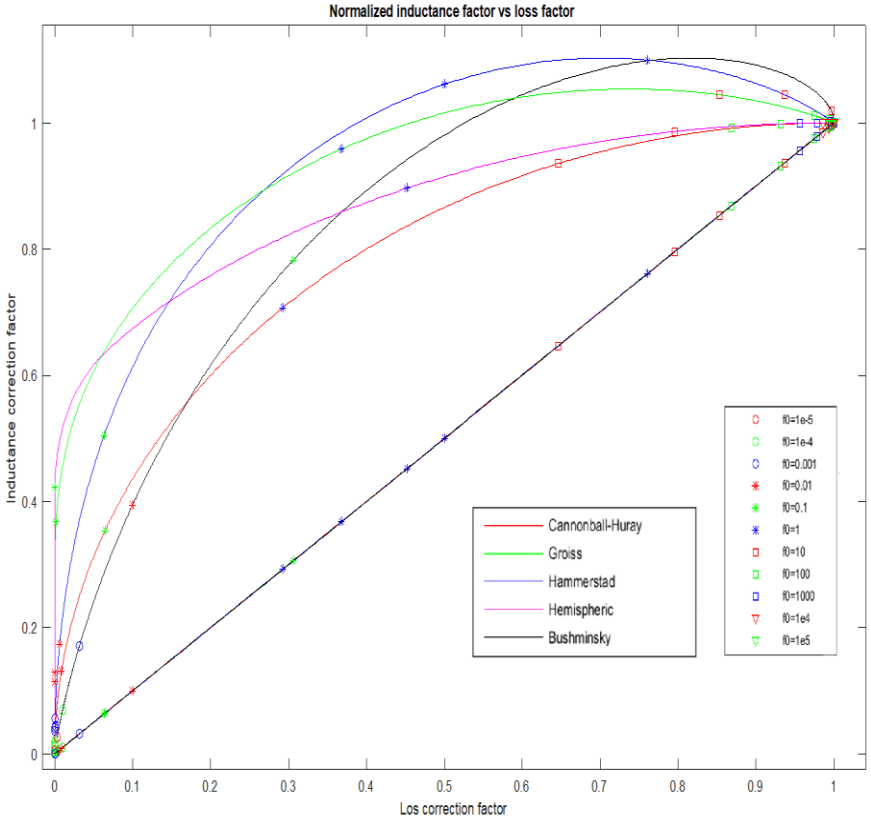

Figure 12. Trajectory showing how loss and inductance correction factors change with frequency. Same denotations as in Fig 11. Trajectories of non-causal models lay on the black straight line

Here, we can clearly see that trajectories of Groiss and Hemispherical models take off vertically, indicating early and considerable onset of the inductive component, when the resistive component remains unobservable. The smoothest onset is in the Bushminsky model; Cannonball-Huray and Hammerstad stay in between. Trajectories of the non-causal versions of all models make a straight line because they assume that inductance correction equals loss correction. We can still follow the progress for non-causal models by following the symbols designating frequency. As expected, causal and non-causal dependencies give the same value of the loss factor at identical frequencies. The vertical distance between the causal and respective non-causal trajectories could be a measure of how much error we introduce when using the non-causal versions of the loss factor. The inductance correction factor grows monotonically in the Cannonball-Huray and Hemispherical models. The Hammerstad, Bushminsky, and to a lesser degree the Groiss model have inductance factor regressing at high frequency.

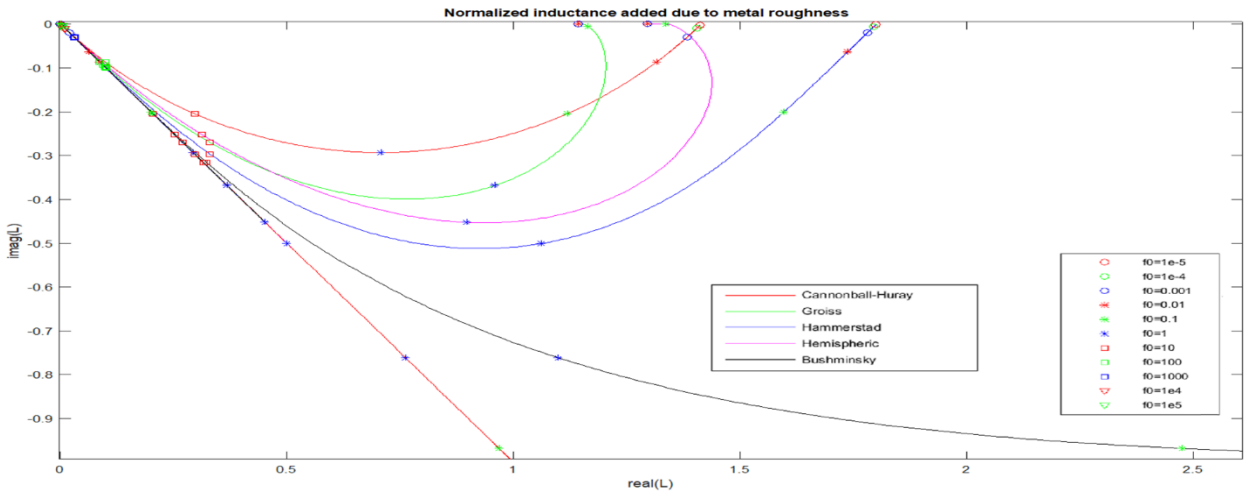

Figure 13. Trajectories of the complex inductance. Same denotations as in Figure 11 and 12

The trajectories of the complex inductance added due to roughness are shown in Figure 13. As causal functions, they curves clockwise, with real part going from right to left. For example, for the Hammestad model (blue) it starts on real axis at coordinates (1.8, 0) then goes down-left, reaches minimum, after which it goes up-left to the origin (0, 0). Similar behavior for Cannonball-Huray (red). The Groiss and Hemispherical models demonstrate some increase in real part of inductance before it begins to decline, without noticeable change in its imaginary part. This behavior is related to the very steep initial growth of the inductance when loss remains small. The Bushminsky model is quite special because its inductance at low frequency is infinite. It starts at (∞, -1), then goes left with real part decreasing as $\log(1/f)$, and imaginary staying close to -1, then joins other trajectories in their move to the origin. Infinite inductance at DC could be overlooked because due to zero limit $\lim_{f\to 0}\left[f\log(1/f)\right]=0$, it brings no extra impedance.

The inductance of *non-causal* models is complex but all trajectories move along the red line connecting points (0, 0) and (1, -1). The movement can be found for all of them by horizontal projection of a causal trajectory on this segment. For all of them - except for Bushminsky – the non-causal inductance starts at the origin, goes down right as imaginary part of the causal model decreases, then then turns and goes back to the origin. For the non-causal Bushminsky model, inductance starts at point (1, -1) and slides up-left to the origin. Certainly, such behavior is physically impossible.

The last in this series is Figure 14 that shows how much extra impedance is added due to metal roughness, when using different models. As we know, due to skin effect, the real and imaginary parts of the impedance of a smooth metal grow as $\sqrt{f}$. In other words, such impedance would go along the black diagonal straight line on Figure 14. The impedance of rough metal, if modeled by a non-causal model, would also belong to the same straight line, although it may grow somewhat faster than $\sqrt{f}$. The additional impedance added due to roughness (but with non-causal models) will be the difference between the latter and the former. Hence, it would also belong to the same diagonal straight line. However, not for the causal models.

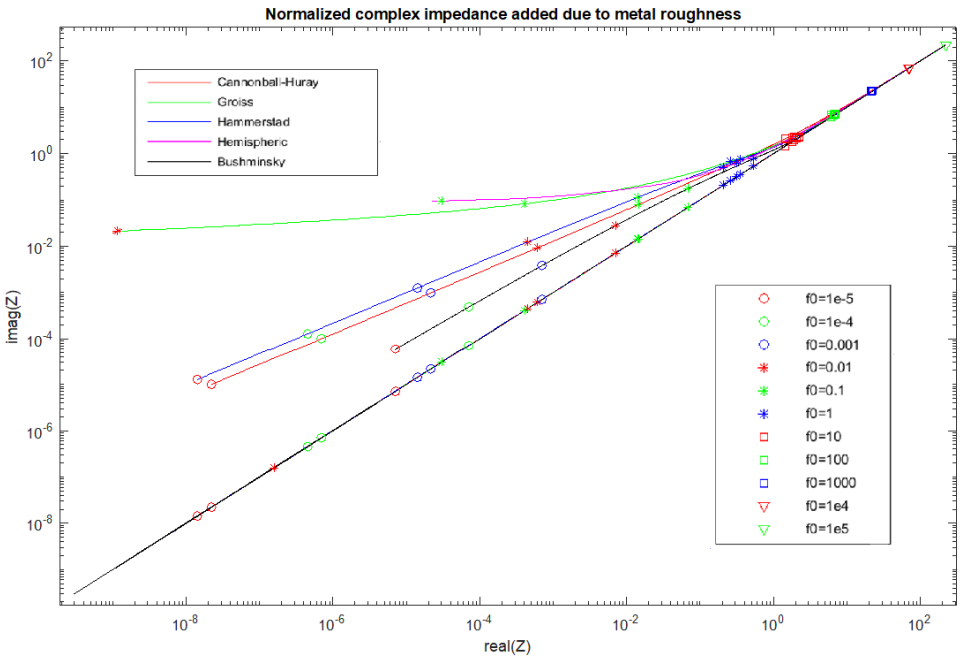

Figure 14. Complex impedance added due to metal roughness. Same denotations as in Figs 11-13. Impedance of all non-causal models belong to the black straight line

As we can see, all causal models add more to the inductive part of the impedance than they do to the resistive, since all their curves lay above the diagonal line. However, the Groiss and Hemispherical models are champions: the ratio between the imaginary and real part of impedance may reach 3-6 orders of magnitude! The Cannonball-Huray and Hammerstad models add considerable inductive portion, too. However, the Bushminsky model seems to add less than the others. Why, if it has infinite inductance at DC? In fact, the outstanding property of the Groiss and Hemispherical models is not in making the largest inductive contribution at a certain frequency, but making it much larger than their contribution to the resistive loss. Indeed, the red star (corresponds to normalized frequency = 0.01) on the Groiss curve is not higher than the corresponding value on the Bushminsky model curve, however, the resistive loss at this frequency in the Groiss model is much smaller. It is a direct consequence of the very steep increase of the inductive factor over the resistive factor that we observed in Figure 9.

Scaling Roughness Factors by Magnitude and Frequency

Of course, in any practical case we need to properly scale the found models by magnitude, and adjust their frequencies considering the actual metal profile. Or, if measured data is available, fit their magnitude and frequency factors to it. Here, we take the example from [4], where the causal Cannonball-Huray roughness model, together with dielectric parameters, has been fitted to measured data. See corresponding insertion loss (IL) curves in Figure 15a, cyan – measured, red – fitted by adjusting the Cannonball model. Parameters of the Cannonball model were calculated assuming $R_z = 3\mu m$ that approximately corresponds to $\Delta_{rms} = 0.85\mu m$. The latter was used for all other standard roughness models (Hammerstad, Groiss, Hemispherical, Bushminsky), which were also adjusted by the magnitude of the loss factor to match the Cannonball model at 50GHz. Loss factors adjusted this way are shown in Figure 15b. The corresponding inductance correction factors are in Figure 15c. They are

larger than loss factors, and have different shapes. Unlike loss correction factors, there exist no single frequency at which all inductance factors become equal.

We can see some similarity between IL and loss factors. For example, the Groiss model (green) has the largest loss factor from 1 to 50 GHz (Figure 15b), which translates into the largest attenuation in Figure 15a. The Cannonball and Hemispherical have the smallest attenuation in this range, which we can observe in the IL plot as well. If some model dominates by the loss factor at a certain frequency, we observe the same effect in the IL plot, too.

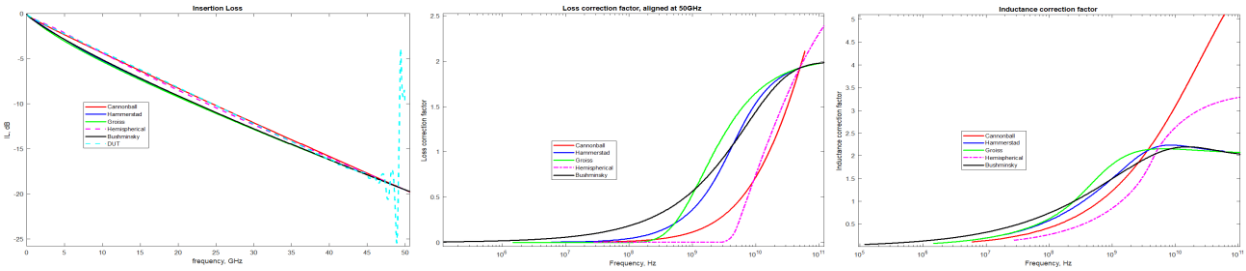

(a) (b) (c)

Figure 15. Insertion loss computed using different roughness models (a); loss correction factors (b); and inductance correction factors (c)

Unlike loss correction, the inductance correction factor mostly affects the phase delay and characteristic impedance, not IL. A larger value of inductance factor means more contribution to the PUL inductance, which increases the phase delay and characteristic impedance. Figures 16a and 16b show the phase delays and the line's TDR impedance plots for all standard models, causal and non-causal.

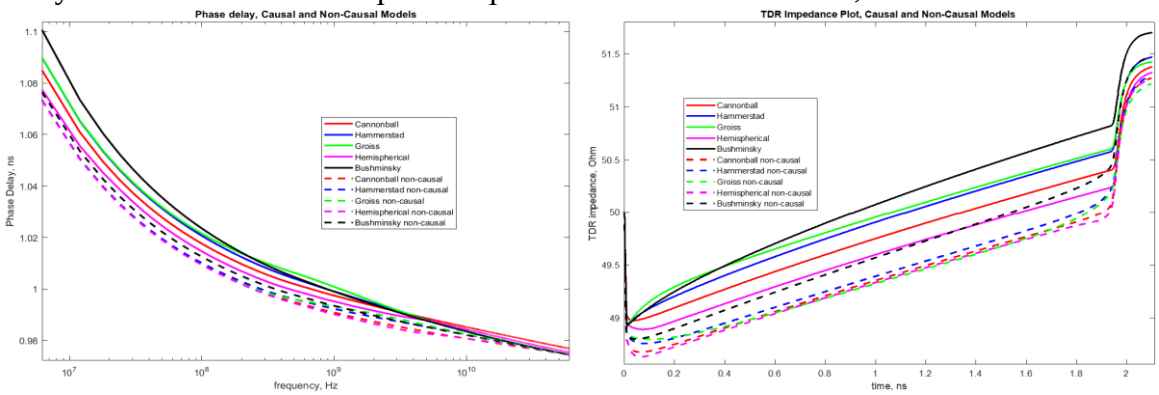

Figure 16. T-line phase delay with different roughness models (a); TDR impedance plots (b). Solid lines represent causal models, dashed – non-causal

For example, the inductance factor in the Bushminsky model is larger than that of the Groiss model approximately up to 250MHz, and so is its phase delay, too. Then, the inductance factor of the Groiss model dominates up to about 3.5GHz, and so does its phase delay, etc. The TDR plot is a function of time, and here we can see dominance by impedance, but in inverse order. During a very short period immediately after start, the Cannonball model (red) creates the largest impedance. Then, between 20 and 400 ps, the largest impedance is shown by the Groiss, and finally by the Bushminsky model. The phase delays and TDR impedances of non-causal versions are always smaller than causal. Also, the order of dominance is defined by their loss correction factor, because it is used as a multiplier for the inductive roughness contribution, too.

How about the infinite inductance of Bushminsky model at DC? Indeed, we can see that it has the largest phase delay at small frequencies and also the largest impedance in "large times". However, an impedance added due to roughness comes to zero together with frequency. Interestingly, the normalized inductance of *non-causal* Bushminsky model remains bounded, because it assumes identical magnitudes for the real and imaginary parts, and so the real part of the normalized inductance at DC would approach 1, not infinity. As we see from Figure 16a, its phase delay plot (dashed black) stays below those from the Groiss, Cannonball and Hemispherical models, which are known to have a finite internal inductance.

To conclude this section, let's note that causal models of metal roughness dependencies are no less diverse as their non-causal counterparts. They also require "adjustment" to match measured dependencies. However, their contributions to the transmission line loss and inductance are different – although not independent – functions of frequency. It is therefore recommended to consider all available dependencies, including insertion loss, phase delay, TDR impedance etc. which depend on both loss and inductance correction factors.

Conclusion

In this paper we proposed a reliable method of restoring the causal complex roughness correction factor from a given dependency that defines loss correction factor. Here, we do not require the loss correction factor to be an analytical function of frequency. It could be a function, but might also be a tabulated frequency dependence found e.g. from measurements. The problem is solved by fitting a known imaginary part of an internal complex inductance with a set of causal basis functions. Such basis functions involve fractional powers of complex frequency, which is dictated by the nature of metal roughness dependencies. We applied this approach to a number of "standard" metal roughness models: Groiss, Hemispherical, Bushminsky, as well as to "custom", which describe the loss correction factor by tables. In all cases, the proposed method helps us to restore causal complex model accurately and reliably. With the full complex dependencies restored, we see that they are more diverse that we would think, considering loss factor alone.

References

[1] A. Djordjevic, R. Biljie, V. Likar-Smiljanic, T. Sarkar, "Wideband frequency domain characterization of FR-4 and time domain causality", IEEE Trans. on EMC, vol.43, No.4, 2001.

[2] Appendix E. "Causal relationship between skin effect resistance and internal inductance for rough conductors," – in [7].

[3] E. Bracken, "A causal Huray model for surface roughness", DesignCon 2012.

[4] V. Dmitriev-Zdorov, Bert Simonovich, I. Kochikov, "A causal conductor roughness model and its effect on transmission line characteristics", DesignCon 2018.

[5] Y. Shlepnev, "Unified approach to interconnect conductor surface roughness modeling", EPEPS, San Jose, CA, 2017

[6] S. Hall, S. Pytel, P. Huray et al. "Multigigahertz causal transmission line modeling methodology using a 3-D hemispherical surface roughness approach," IEEE Trans. on Microwave Theory and Techniques, v.55, No.12, 2007

[7] S. Hall, H. Heck, "Advanced signal integrity for high speed digital designs," John Willey & Sons Inc., Hoboken, NJ, 2009.

[8] K. Oldham, J. Spanier, “The fractional calculus: integrations and differentiations of arbitrary order”, New York: Academic Press, 1974
[9] K. Miller, B. Ross, “An Introduction to the Fractional Calculus and Fractional Differential Equations”, John Wiley & Sons, 1993.
[10] G. Folland, Advanced Calculus, Prentice Hall (2002)
[11] S. Groiss, et al, “Parameters of loss cavity resonators calculated by the finite element method”, IEEE Trans. on Magnetism, v.32, No 3, May 1996.
[12] E. Hammerstad, O. Jensen, “Accurate models for microstrip computer-aided design”, IEEE-MTT-S Int. Microwave Symp. Digest, May 1980
[13] P. Huray, “The foundations of signal integrity,” John Willey & Sons Inc., Hoboken, NJ, 2009.
[14] E. Bogatin, D. DeGroot, P. Huray, and Y. Shlepnev, “Which one is better? Comparing options to describe frequency dependent losses,” DesignCon 2013.
[15] Y. Shlepnev, “Modeling frequency-dependent dielectric loss and dispersion for multigigabit data channels”, Simbeor Application Note 2008.
[16] Simberian Inc., 3030 S Torrey Pines Dr. Las Vegas, NV 89146, USA. URL: http://www.simberian.com/
[17] Wild River Technology LLC 8311 SW Charlotte Drive Beaverton, OR 97007. URL: https://wildrivertech.com/
[18] B. Simonovich, "Practical model of conductor surface roughness using cubic close-packing of equal spheres", EDICon 2016
[19] A. F. Horn, J. W. Reynolds and J. C. Rautio, "Conductor profile effects on the propagation constant of microstrip transmission lines," Microwave Symposium Digest (MTT), 2010 IEEE MTT-S International, Anaheim, CA, 2010, pp. 1-1.doi: 10.1109/MWSYM.2010.5517477
[20] B. Simonovich, "A practical method to model effective permittivity and phase delay due to conductor surface roughness", DesignCon 2017